

# A note on transformed Fourier systems for the approximation of non-periodic signals

Robert Nasdala<sup>1</sup>      Daniel Potts<sup>2</sup>

A variety of techniques have been developed for the approximation of non-periodic functions. In particular, there are approximation techniques based on rank-1 lattices and transformed rank-1 lattices, including methods that use sampling sets consisting of Chebyshev- and tent-transformed nodes. We compare these methods with a parameterized transformed Fourier system that yields similar  $\ell_2$ -approximation errors.

Keywords and phrases : approximation on the high dimensional cube, change of variables, lattice rule, rank-1 lattice, fast Fourier transform

2010 AMS Mathematics Subject Classification : 65T 42B05

## 1 Introduction

For the approximation of non-periodic functions defined on the cube  $[0, 1]^d$ , fast algorithms based on Chebyshev- and tent-transformed rank-1 lattice methods have been introduced in [15, 9]. Recently, we suggested a general framework for transformed rank-1 lattice approximation, in which functions defined on the cube  $[-\frac{1}{2}, \frac{1}{2}]^d$  are periodized onto  $\mathbb{R}^d$  or  $\mathbb{T}^d$ , [10, 11]. In these approaches we define parameterized families  $\psi(\circ, \boldsymbol{\eta}) : [0, 1]^d \rightarrow [0, 1]^d$ ,  $\boldsymbol{\eta} \in \mathbb{R}_+^d$  of transformations that, depending on the parameter choice, yield a certain smoothening effect when composed with a given non-periodic function. This periodization strategies also lead to general parameterized classes of orthonormal systems in weighted Hilbert spaces. However, these methods have the natural drawback of singularities appearing at the boundary points of the cube, so that any approximation error estimates have to be done with respect to weighted  $L_\infty$ - and  $L_2$ -norms.

We reflect some crucial properties of rank-1 lattice approximation. Then, we compare the Chebyshev approximation, the approximation with a half-periodic cosine system and tent-transformed sampling nodes, as well as the general framework for the parameterized transformed Fourier system. We discuss numerical results in up to dimension  $d = 3$  and highlight the controlled smoothening effect when varying the parameter  $\boldsymbol{\eta}$  in the transformed Fourier systems.

---

<sup>1</sup>Faculty of Mathematics, Chemnitz University of Technology, D-09107 Chemnitz, Germany.  
E-mail: robert.nasdala@math.tu-chemnitz.de

<sup>2</sup>Faculty of Mathematics, Chemnitz University of Technology, D-09107 Chemnitz, Germany.  
E-mail: potts@math.tu-chemnitz.de

## 2 Approximation methods

At first we reflect the main ideas of the Fourier approximation with sampling sets in the form of rank-1 lattices [14, 4, 8]. We consider Chebyshev- and tent-transformed rank-1 lattices in the context of Chebyshev and cosine approximation methods [15, 9]. Finally, we outline the transformed Fourier system for the approximation of non-periodic signals, as introduced in [11], and provide two examples of parameterized transformations.

### 2.1 Fourier approximation

For any frequency set  $I \subset \mathbb{Z}^d$  of finite cardinality  $|I| < \infty$  we denote the space of all multivariate trigonometric polynomials supported on  $I$  by

$$\Pi_I := \text{span} \left\{ e^{2\pi i \mathbf{k} \cdot \circ} = \prod_{j=1}^d e^{2\pi i k_j \circ} : \mathbf{k} \in I \right\},$$

which forms an orthonormal system with respect to the  $L_2(\mathbb{T}^d)$ -scalar product

$$(f, g)_{L_2(\mathbb{T}^d)} := \int_{\mathbb{T}^d} f(\mathbf{x}) \overline{g(\mathbf{x})} d\mathbf{x}, \quad f, g \in L_2(\mathbb{T}^d).$$

For all  $\mathbf{k} \in \mathbb{Z}^d$  we denote the *Fourier coefficients*  $\hat{h}_{\mathbf{k}}$  by

$$\hat{h}_{\mathbf{k}} := (h, e^{2\pi i \mathbf{k} \cdot \circ})_{L_2(\mathbb{T}^d)} = \int_{\mathbb{T}^d} h(\mathbf{x}) e^{-2\pi i \mathbf{k} \cdot \mathbf{x}} d\mathbf{x},$$

and the corresponding *Fourier partial sum* by  $S_I h(\mathbf{x}) := \sum_{\mathbf{k} \in I} \hat{h}_{\mathbf{k}} e^{2\pi i \mathbf{k} \cdot \mathbf{x}}$ .

We use sampling nodes in a *rank-1 lattice*  $\Lambda(\mathbf{z}, M)$  of size  $M \in \mathbb{N}$  generated by the vector  $\mathbf{z} \in \mathbb{Z}^d$ , that is defined as

$$\Lambda(\mathbf{z}, M) := \left\{ \mathbf{x}_j^{\text{latt}} := \frac{j}{M} \mathbf{z} \pmod{\mathbf{1}} \in \mathbb{T}^d : j = 0, \dots, M-1 \right\}, \quad (2.1)$$

which allows the fast evaluation of Fourier partial sums via [8, Algorithm 3.1]. For any frequency set  $I \subset \mathbb{Z}^d$  the *difference set* is given by

$$\mathcal{D}(I) := \{\mathbf{k} \in \mathbb{Z}^d : \mathbf{k} = \mathbf{k}_1 - \mathbf{k}_2 \text{ with } \mathbf{k}_1, \mathbf{k}_2 \in I\}.$$

We define the *reconstructing rank-1 lattice*  $\Lambda(\mathbf{z}, M, I)$  as a rank-1 lattice  $\Lambda(\mathbf{z}, M)$  for which the condition

$$\mathbf{t} \cdot \mathbf{z} \not\equiv 0 \pmod{M} \quad \text{for all } \mathbf{t} \in \mathcal{D}(I) \setminus \{\mathbf{0}\} \quad (2.2)$$

holds. Given a reconstructing rank-1 lattice  $\Lambda(\mathbf{z}, M, I)$ , we have exact integration for all multivariate trigonometric polynomials  $p \in \Pi_{\mathcal{D}(I)}$ , see [14], so that

$$\int_{\mathbb{T}^d} p(\mathbf{x}) d\mathbf{x} = \frac{1}{M} \sum_{j=0}^{M-1} p(\mathbf{x}_j), \quad \mathbf{x}_j \in \Lambda(\mathbf{z}, M, I).$$

In particular, for  $h \in \Pi_I$  and  $\mathbf{k} \in I$  we have  $h(\circ) e^{-2\pi i \mathbf{k} \cdot \circ} \in \Pi_{\mathcal{D}(I)}$  and

$$\hat{h}_{\mathbf{k}} = \int_{\mathbb{T}^d} h(\mathbf{x}) e^{-2\pi i \mathbf{k} \cdot \mathbf{x}} d\mathbf{x} = \frac{1}{M} \sum_{j=0}^{M-1} h(\mathbf{x}_j) e^{-2\pi i \mathbf{k} \cdot \mathbf{x}_j}, \quad \mathbf{x}_j \in \Lambda(\mathbf{z}, M, I). \quad (2.3)$$

Next, we focus on functions in the Wiener algebra  $\mathcal{A}(\mathbb{T}^d)$  containing all  $L_1(\mathbb{T}^d)$ -functions with absolutely summable Fourier coefficients. For an arbitrary function  $h \in \mathcal{A}(\mathbb{T}^d) \cap \mathcal{C}(\mathbb{T}^d)$  and lattice points  $\mathbf{x}_j \in \Lambda(\mathbf{z}, M, I)$  we lose the former mentioned exact integration property and get *approximated Fourier coefficients*  $\hat{h}_{\mathbf{k}}^\Lambda$  of the form

$$\hat{h}_{\mathbf{k}} \approx \hat{h}_{\mathbf{k}}^\Lambda := \frac{1}{M} \sum_{j=0}^{M-1} h(\mathbf{x}_j) e^{-2\pi i \mathbf{k} \cdot \mathbf{x}_j}$$

leading to the *approximated Fourier partial sum*  $S_I^\Lambda f$  given by

$$h(\mathbf{x}) \approx S_I^\Lambda h(\mathbf{x}) := \sum_{\mathbf{k} \in I} \hat{h}_{\mathbf{k}}^\Lambda e^{2\pi i \mathbf{k} \cdot \mathbf{x}}.$$

For the matrix-vector-expression with respect to the frequency set  $I_{\text{latt}} \subset \mathbb{Z}^d$  we put

$$\mathbf{F}_{\text{latt}} := \left\{ e^{2\pi i \mathbf{k} \cdot \mathbf{x}_j^{\text{latt}}} \right\}_{j=0, \mathbf{k} \in I_{\text{latt}}}^{M-1}, \quad \mathbf{h}_{\text{latt}} := \left( h(\mathbf{x}_j^{\text{latt}}) \right)_{j=0}^{M-1}.$$

The evaluation of the function  $h$  and the reconstruction of the approximated Fourier coefficients  $\hat{\mathbf{h}} := (\hat{h}_{\mathbf{k}}^\Lambda)_{\mathbf{k} \in I_{\text{latt}}}$  are realized by the fast Algorithms outlined in [8, Algorithm 3.1 and 3.2] that compute the systems

$$\mathbf{h}_{\text{latt}} = \mathbf{F}_{\text{latt}} \hat{\mathbf{h}} \quad \text{and} \quad \hat{\mathbf{h}} = \mathbf{F}_{\text{latt}}^* \mathbf{h}_{\text{latt}}. \quad (2.4)$$

## 2.2 Chebyshev approximation

We consider the Chebyshev system, that is defined for  $\mathbf{x} = (x_1, \dots, x_d)^\top \in [0, 1]^d$  and a finite frequency set  $\mathbf{k} = (k_1, \dots, k_d)^\top \in I_{\text{cheb}} \subset \mathbb{N}_0^d$  as

$$\left\{ T_{\mathbf{k}}(\mathbf{x}) := \prod_{\ell=1}^d \sqrt{2}^{1-\delta_{k_\ell, 0}} \cos(k_\ell \arccos(2x_\ell - 1)) \right\}_{\mathbf{k} \in I_{\text{cheb}}} \quad (2.5)$$

and is an orthonormal system with respect to the weighted scalar product

$$(T_{\mathbf{k}_1}, T_{\mathbf{k}_2})_{L_2, \omega}([0, 1]^d) := \int_{[0, 1]^d} T_{\mathbf{k}_1}(\mathbf{x}) \overline{T_{\mathbf{k}_2}(\mathbf{x})} \omega(\mathbf{x}) d\mathbf{x}, \quad \omega(\mathbf{x}) := \prod_{j=1}^d \frac{2}{\pi \sqrt{4x_j(1-x_j)}}.$$

We transfer some properties of the Fourier system via the *Chebyshev transformation*

$$\psi(\mathbf{x}) := (\psi_1(x_1), \dots, \psi_d(x_d))^\top, \quad \psi_j(x_j) := \frac{1}{2} + \frac{1}{2} \cos(\pi x_j), \quad x_j \in [0, 1]. \quad (2.6)$$

We note that Chebyshev transformed sampling nodes are fundamentally connected to Padua points and Lissajous curves, as well as certain interpolation methods that are outlined in [1, 6].

The *Chebyshev coefficients* of an  $h \in L_{2,\omega}([0,1]^d)$  are given by  $\hat{c}_{\mathbf{k}} := (h, T_{\mathbf{k}})_{L_{2,\omega}([0,1]^d)}$ ,  $\mathbf{k} \in \mathbb{Z}^d$ . We have sampling nodes in the Chebyshev-transformed rank-1 lattice  $\Lambda_{\psi}(\mathbf{z}, M)$  defined as

$$\Lambda_{\psi}(\mathbf{z}, M) := \left\{ \mathbf{x}_j^{\text{cheb}} := \psi \left( \mathbf{x}_j^{\text{latt}} \right) : \mathbf{x}_j^{\text{latt}} \in \Lambda(\mathbf{z}, M), j = 0, \dots, M-1 \right\}. \quad (2.7)$$

It inherits the reconstruction property (2.2) of the underlying reconstructing rank-1 lattice  $\Lambda(\mathbf{z}, M, I)$  and is denoted by  $\Lambda_{\psi}(\mathbf{z}, M, I)$ .

Furthermore, the multivariate Chebyshev polynomials supported on  $I \subset \mathbb{Z}^d$  are given by  $\Pi_I^{\text{cheb}} := \text{span}\{T_{\mathbf{k}} : \mathbf{k} \in I\}$  and have the exact integration property (2.3). Hence, for  $h \in \Pi_I^{\text{cheb}}$  we have

$$\hat{c}_{\mathbf{k}} = \int_{[0,1]^d} h(\mathbf{x}) T_{\mathbf{k}}(\mathbf{x}) \omega(\mathbf{x}) \, d\mathbf{x} = \frac{1}{M} \sum_{j=0}^{M-1} h(\mathbf{x}_j) T_{\mathbf{k}}(\mathbf{x}_j^{\text{cheb}}), \quad \mathbf{x}_j^{\text{cheb}} \in \Lambda_{\psi}(\mathbf{z}, M, I),$$

which yields *approximated Chebyshev coefficients* of the form

$$\hat{c}_{\mathbf{k}}^{\Lambda} := \frac{1}{M} \sum_{j=0}^{M-1} h(\mathbf{x}_j) T_{\mathbf{k}}(\mathbf{x}_j^{\text{cheb}})$$

and leads to the *approximated Chebyshev partial sum*  $S_I^{\Lambda} f$  given by

$$h(\mathbf{x}) \approx S_I^{\Lambda} h(\mathbf{x}) := \sum_{\mathbf{k} \in I} \hat{c}_{\mathbf{k}}^{\Lambda} T_{\mathbf{k}}(\mathbf{x}). \quad (2.8)$$

In matrix-vector-notation this reads as

$$\mathbf{T}_{\text{cheb}} := \left\{ T_{\mathbf{k}}(\mathbf{x}_j^{\text{cheb}}) \right\}_{j=0, \mathbf{k} \in I_{\text{cheb}}}^{M-1}, \quad \mathbf{h}_{\text{cheb}} := \left( h(\mathbf{x}_j^{\text{cheb}}) \right)_{j=0}^{M-1}.$$

The evaluation of  $h$  as well as the reconstruction of the approximated Chebyshev coefficients  $\hat{\mathbf{c}} := (\hat{c}_{\mathbf{k}}^{\Lambda})_{\mathbf{k} \in I_{\text{cheb}}}$  of  $h$  are realized by fast Algorithms outlined in [15, 12, 9], that compute the systems

$$\mathbf{h}_{\text{cheb}} = \mathbf{T}_{\text{cheb}} \hat{\mathbf{c}} \quad \text{and} \quad \hat{\mathbf{c}} = \mathbf{T}_{\text{cheb}}^* \mathbf{h}_{\text{cheb}}. \quad (2.9)$$

## 2.3 Cosine approximation

Next, we consider the half-periodic cosine system

$$\left\{ \lambda_{\mathbf{k}}(\circ) := \sqrt{2}^{|\mathbf{k}|_0} \prod_{j=1}^d \cos(\pi k_j \circ) \right\}_{\mathbf{k} \in I_{\text{tent}}}, \quad I_{\text{tent}} \subset \mathbb{N}_0^d. \quad (2.10)$$

In [7] it is pointed out that this system can alternatively be defined in one dimension over the domain  $t \in [-1, 1]$  as the system  $\lambda_0(x) = \frac{1}{\sqrt{2}}$ ,  $\lambda_k(t) = \cos(k\pi t)$ ,  $\tilde{\lambda}_k(t) = \sin((k - \frac{1}{2})\pi t)$ , which yields the original cosine system after applying the transformation  $t = 2x - 1$ .

The cosine system (2.10) is orthonormal with respect to the  $L_2([0, 1]^d)$ -scalar product and the cosine coefficients of a function  $h \in L_2([0, 1]^d)$  are given by  $\hat{g}_{\mathbf{k}} := (h, \lambda_{\mathbf{k}})_{L_2([0, 1]^d)}$ . We transfer the crucial properties of the Fourier system via the tent transformation

$$\psi(\mathbf{x}) := (\psi_1(x_1), \dots, \psi_d(x_d))^\top, \quad \psi_j(x_j) = \begin{cases} 2x_j & \text{for } 0 \leq x_j < \frac{1}{2}, \\ 2 - 2x_j & \text{for } \frac{1}{2} \leq x_j \leq 1. \end{cases} \quad (2.11)$$

We have sampling nodes in the tent-transformed rank-1 lattice  $\Lambda_\psi(\mathbf{z}, M)$  defined as

$$\Lambda_\psi(\mathbf{z}, M) := \left\{ \mathbf{x}_j^{\text{tent}} := \psi \left( \mathbf{x}_j^{\text{latt}} \right) : \mathbf{x}_j^{\text{latt}} \in \Lambda(\mathbf{z}, M), j = 0, \dots, M-1 \right\} \quad (2.12)$$

and we speak of a reconstructing tent-transformed rank-1 lattice  $\Lambda_\psi(\mathbf{z}, M, I)$  if the underlying rank-1 lattice is a reconstructing one. Furthermore, the multivariate cosine polynomials supported on  $I \subset \mathbb{Z}^d$  are given by  $\Pi_I^{\text{tent}} := \text{span}\{\lambda_{\mathbf{k}} : \mathbf{k} \in I\}$  and inherit the exact integration property (2.3). Thus, for  $h \in \Pi_I^{\text{tent}}$  we have

$$\hat{g}_{\mathbf{k}} = \int_{[0, 1]^d} h(\mathbf{x}) \lambda_{\mathbf{k}}(\mathbf{x}) \, d\mathbf{x} = \frac{1}{M} \sum_{j=0}^{M-1} h(\mathbf{x}_j) \lambda_{\mathbf{k}}(\mathbf{x}_j^{\text{tent}}), \quad \mathbf{x}_j^{\text{tent}} \in \Lambda_\psi(\mathbf{z}, M, I),$$

which yields *approximated cosine coefficients* of the form

$$\hat{g}_{\mathbf{k}}^\Lambda := \frac{1}{M} \sum_{j=0}^{M-1} h(\mathbf{x}_j) \lambda_{\mathbf{k}}(\mathbf{x}_j^{\text{tent}})$$

and leads to the *approximated cosine partial sum*  $S_I^\Lambda f$  given by

$$h(\mathbf{x}) \approx S_I^\Lambda h(\mathbf{x}) := \sum_{\mathbf{k} \in I} \hat{h}_{\mathbf{k}}^\Lambda \lambda_{\mathbf{k}}(\mathbf{x}). \quad (2.13)$$

In matrix-vector-notation we have

$$\mathbf{h}_{\text{tent}} := (h(\mathbf{x}_j^{\text{tent}}))_{j=0}^{M-1}, \quad \mathbf{C}_{\text{tent}} := \{\lambda_{\mathbf{k}}(\mathbf{x}_j^{\text{tent}})\}_{j=0, \mathbf{k} \in I_{\text{tent}}}^{M-1}.$$

Both the evaluation of  $h$  and the reconstruction of the approximated cosine coefficients  $\hat{\mathbf{g}} := \{\hat{g}_{\mathbf{k}}^\Lambda\}_{\mathbf{k} \in I_{\text{tent}}}$  is realized by solving the systems

$$\mathbf{h}_{\text{tent}} = \mathbf{T}_{\text{tent}} \hat{\mathbf{g}}, \quad \text{and} \quad \hat{\mathbf{g}} = \mathbf{T}_{\text{tent}}^* \mathbf{h}_{\text{tent}}. \quad (2.14)$$

Fast algorithms for the computation of both systems are described in [15, 9].

## 2.4 Transformed Fourier approximation

We reflect the ideas of a particular family of parameterized torus-to-cube transformations as suggested in [10, 11], that generalize the construction idea of the Chebyshev system in composing a mapping with a multiple of its inverse.

We call a continuously differentiable, increasing and odd mapping  $\tilde{\psi} : (0, 1) \rightarrow \mathbb{R}$  with  $\tilde{\psi}(x) \rightarrow \pm\infty$  for  $x \rightarrow \{0, 1\}$  a *transformation to  $\mathbb{R}$* . We obtain a parameterized *torus-to-cube transformation*  $\psi(\cdot, \eta) : [0, 1] \rightarrow [0, 1]$  with  $\eta \in \mathbb{R}_+ := (0, \infty)$  by putting

$$\psi(x, \eta) := \begin{cases} 0 & \text{for } x = 0, \\ \tilde{\psi}^{-1}(\eta \tilde{\psi}(x)) & \text{for } x \in (0, 1), \\ 1 & \text{for } x = 1, \end{cases} \quad (2.15)$$

which are continuously differentiable, increasing and have a first derivative  $\psi'(\circ, \boldsymbol{\eta}) \in \mathcal{C}(\mathbb{T})$ . It holds  $\psi^{-1}(y, \boldsymbol{\eta}) = \psi\left(y, \frac{1}{\boldsymbol{\eta}}\right)$  and we call  $\varrho(y, \boldsymbol{\eta}) := (\psi^{-1})'(y, \boldsymbol{\eta}) = \psi'\left(y, \frac{1}{\boldsymbol{\eta}}\right)$  the *density of  $\psi$* . In multiple dimensions  $d \in \mathbb{N}$  with  $\boldsymbol{\eta} = (\eta_1, \dots, \eta_d)^\top$  we put

$$\begin{aligned}\psi(\mathbf{x}, \boldsymbol{\eta}) &:= (\psi_1(x_1, \eta_1), \dots, \psi_d(x_d, \eta_d))^\top, \\ \psi^{-1}(\mathbf{y}, \boldsymbol{\eta}) &:= (\psi_1^{-1}(y_1, \eta_1), \dots, \psi_d^{-1}(y_d, \eta_d))^\top, \\ \varrho(\mathbf{y}, \boldsymbol{\eta}) &:= \prod_{j=1}^d \varrho_j(y_j, \eta_j) \quad \text{with} \quad \varrho(y_j, \eta_j) := \frac{1}{\psi'(\psi^{-1}(y_j, \eta_j))}.\end{aligned}$$

Applying a torus-to-cube transformation to a function  $h \in L_{2,\omega}([0,1]^d)$  generates a periodic function  $f \in L_2(\mathbb{T}^d)$  of the form

$$f(\mathbf{x}) := h(\psi(\mathbf{x}, \boldsymbol{\eta})) \sqrt{\omega(\psi(\mathbf{x}, \boldsymbol{\eta})) \prod_{j=1}^d \psi'_j(x_j)} \quad \text{with} \quad \|h\|_{L_{2,\omega}([0,1]^d)} = \|f\|_{L_2(\mathbb{T}^d)}, \quad (2.16)$$

that is approximated by the classical Fourier system. To construct an approximant for the original function  $h$  we apply the inverse torus-to-cube transformation to the Fourier system, yielding the *transformed Fourier system*

$$\left\{ \varphi_{\mathbf{k}}(\circ, \boldsymbol{\eta}) := \sqrt{\frac{\varrho(\circ, \boldsymbol{\eta})}{\omega(\circ)}} e^{2\pi i \mathbf{k} \cdot \psi^{-1}(\circ, \boldsymbol{\eta})} \right\}_{\mathbf{k} \in I}, \quad (2.17)$$

which forms an orthonormal system with respect to the weighted  $L_{2,\omega}([0,1]^d)$ -scalar product. For all  $\mathbf{k} \in \mathbb{Z}^d$  the *transformed Fourier coefficients*  $\hat{h}_{\mathbf{k}}$  are naturally defined as

$$\hat{h}_{\mathbf{k}} := (h, \varphi_{\mathbf{k}}(\circ, \boldsymbol{\eta}))_{L_{2,\omega}([0,1]^d)} = \int_{[0,1]^d} h(\mathbf{x}) \varphi_{\mathbf{k}}(\mathbf{x}, \boldsymbol{\eta}) \omega(\mathbf{x}) \, d\mathbf{x},$$

and the corresponding *Fourier partial sum* is given by  $S_I h(\mathbf{x}) := \sum_{\mathbf{k} \in I} \hat{h}_{\mathbf{k}} \varphi_{\mathbf{k}}(\mathbf{x}, \boldsymbol{\eta})$ . The corresponding sampling nodes will be taken from the torus-to-cube-transformed (abbreviated: ttc) rank-1 lattice  $\Lambda_\psi(\mathbf{z}, M)$  defined as

$$\Lambda_\psi(\mathbf{z}, M) := \left\{ \mathbf{x}_j^{\text{ttc}} := \psi\left(\mathbf{x}_j^{\text{latt}}, \boldsymbol{\eta}\right) : \mathbf{x}_j^{\text{latt}} \in \Lambda(\mathbf{z}, M), j = 0, \dots, M-1 \right\} \quad (2.18)$$

and we speak of a reconstructing torus-to-cube-transformed rank-1 lattice  $\Lambda_\psi(\mathbf{z}, M, I)$  if the underlying rank-1 lattice is a reconstructing one.

Furthermore, the multivariate transformed trigonometric polynomials supported on  $I \subset \mathbb{Z}^d$  are given by  $\Pi_I^{\text{ttc}} := \text{span}\{\varphi_{\mathbf{k}} : \mathbf{k} \in I\}$  and inherit the exact integration property (2.3), thus, for  $h \in \Pi_I^{\text{ttc}}$  we have

$$\hat{h}_{\mathbf{k}} = \int_{[0,1]^d} h(\mathbf{x}) \varphi_{\mathbf{k}}(\mathbf{x}) \, d\mathbf{x} = \frac{1}{M} \sum_{j=0}^{M-1} h(\mathbf{x}_j) \varphi_{\mathbf{k}}(\mathbf{x}_j^{\text{ttc}}), \quad \mathbf{x}_j^{\text{ttc}} \in \Lambda_\psi(\mathbf{z}, M, I),$$

which yields approximated cosine coefficients of the form

$$\hat{h}_{\mathbf{k}}^\Lambda := \frac{1}{M} \sum_{j=0}^{M-1} h(\mathbf{x}_j) \varphi_{\mathbf{k}}(\mathbf{x}_j^{\text{ttc}})$$

and leads to the *approximated transformed Fourier partial sum*  $S_I^\Lambda f$  given by

$$h(\mathbf{x}) \approx S_I^\Lambda h(\mathbf{x}) := \sum_{\mathbf{k} \in I} \hat{h}_{\mathbf{k}}^\Lambda \varphi_{\mathbf{k}}(\mathbf{x}, \boldsymbol{\eta}). \quad (2.19)$$

In matrix-vector-notation we have

$$\mathbf{h}_{\text{ttc}} := (h(\mathbf{x}_j^{\text{ttc}}))_{j=0}^{M-1}, \quad \mathbf{F}_{\text{ttc}} := \{\varphi_{\mathbf{k}}(\mathbf{x}_j^{\text{ttc}})\}_{j=0, \mathbf{k} \in I_{\text{ttc}}}^{M-1}.$$

The evaluation of  $h$  and the reconstruction of the approximated transformed Fourier coefficients  $\hat{\mathbf{h}} := \{\hat{h}_{\mathbf{k}}^\Lambda\}_{\mathbf{k} \in I_{\text{ttc}}}$  is realized by solving the systems

$$\mathbf{h}_{\text{ttc}} = \mathbf{F}_{\text{ttc}} \hat{\mathbf{h}}, \quad \text{and} \quad \hat{\mathbf{h}} = \mathbf{F}_{\text{ttc}}^* \mathbf{h}_{\text{ttc}}. \quad (2.20)$$

Fast algorithms for the computation of both systems are described in [11].

## 2.5 Comparison of the orthonormal systems

The previously presented approximation approaches are based on very different orthonormal systems and use differently transformed sampling sets, which is summarized in dimension  $d = 1$  in Table 2.1 with the definition of the hyperbolic cross  $I_N^d$  given in (3.4).

Applying the univariate tent-transformation (2.11) to a sampling set of equispaced nodes, can be interpreted as mirroring the given function at its right boundary point and approximating the resulting function by means of a half-periodic cosine system. However, the produced continuous periodic function generally won't be smooth.

The invertible Chebyshev-transformation (2.6) mirrors the original function and additionally smoothens it at the boundary points, leading to better approximation results. The also invertible parametrized torus-to-cube transformation (2.15) adapts the idea of the Chebyshev-transformation by mirroring the original function into an even, continuous and periodic function. Additionally, the involved parameter  $\boldsymbol{\eta}$  controls the smoothing effect on the periodized function, see [11].

**Example 2.1.** We find various suggestions for transformations to  $\mathbb{R}$  in [2, Section 17.6], [13, Section 7.5] and [10]. We list some induced combined transformations  $\psi(x, \eta)$  and the corresponding density function  $\varrho(y, \eta) = (\psi^{-1})'(y, \eta)$  in the sense of definition (2.15):

- the logarithmic torus-to-cube transformation

$$\psi(x, \eta) := \frac{1}{2} + \frac{1}{2} \tanh(\eta \tanh^{-1}(2x - 1)), \quad \varrho(y, \eta) = \frac{4}{\eta} \frac{(4y - 4y^2)^{\frac{1}{\eta} - 1}}{\left((2y)^{\frac{1}{\eta}} + (2 - 2y)^{\frac{1}{\eta}}\right)^2}, \quad (2.21)$$

based on the mapping

$$\tilde{\psi}(x) = \frac{1}{2} \log \left( \frac{2x}{2 - 2x} \right) = \tanh^{-1}(2x - 1),$$

- the error function torus-to-cube transformation

$$\psi(x, \eta) = \frac{1}{2} \operatorname{erf}(\eta \operatorname{erf}^{-1}(2x - 1)) + \frac{1}{2}, \quad \varrho(y, \eta) = \frac{1}{\eta} e^{(1 - \frac{1}{\eta^2})(\operatorname{erf}^{-1}(2y - 1))^2}, \quad (2.22)$$

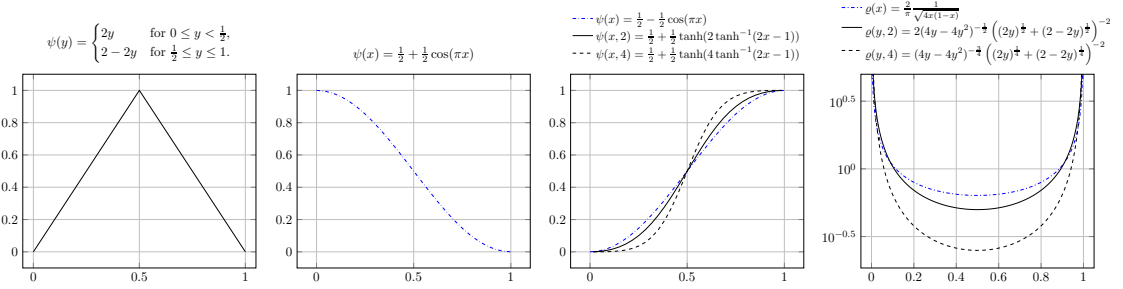


Figure 2.1: Left: The tent-transformation (2.11). Left-center: The Chebyshev-transformation (2.6). Right-center: The parameterized logarithmic transformation (2.21) in comparison with the mirrored Chebyshev-transformation. Right: The density functions of the parameterized logarithmic transformation (2.21) in comparison with the mirrored Chebyshev-transformation.

orthonormal system $\{\varphi_k(x)\}_{k \in I}$	scalar product weight $\omega$	sampling transformation $\psi$	frequency set $I$
$\sqrt{2}^{\ k\ _0} \cos(\pi k x)$	1	$\begin{cases} 2x & \text{for } 0 \leq x < \frac{1}{2}, \\ 2-2x & \text{for } \frac{1}{2} \leq x \leq 1. \end{cases}$	$I_N^d \cap \mathbb{N}_0^d$
$\sqrt{2}^{1-\delta_{k,0}} \cos(k \arccos(2x-1))$	$\frac{2}{\pi \sqrt{4x(1-x)}}$	$\frac{1}{2} + \frac{1}{2} \cos(\pi x)$	$I_N^d \cap \mathbb{N}_0^d$
$\sqrt{\frac{\varrho(x, \eta)}{\omega(x)}} e^{2\pi i k \psi^{-1}(x, \eta)}$	$\omega(x)$	$\psi(x, \eta)$	$I_N^d$

Table 2.1: Comparison of the univariate orthonormal system, sampling sets and frequency sets from the Chebyshev, Cosine and transformed Fourier approximation methods.

based on the mapping

$$\tilde{\psi}(x) = \operatorname{erf}^{-1}(2x-1),$$

which is the inverse of the error function

$$\operatorname{erf}(y) = \frac{1}{\sqrt{\pi}} \int_{-y}^y e^{-t^2} dt, \quad y \in \mathbb{R},$$

□

In Figure 2.1 we provide a side-by-side comparison of all the previously mentioned transformation mappings. Furthermore, the right plot of Figure 2.1 highlights how increasing the parameter  $\eta$  leads to smoother transformations  $\psi(\circ, \eta)$  than the Chebyshev transformation. Furthermore, the transformed Fourier system requires a symmetric frequency set, such as the hyperbolic cross (3.4), in contrast to both the cosine and the Chebyshev systems only requires non-negative frequencies.



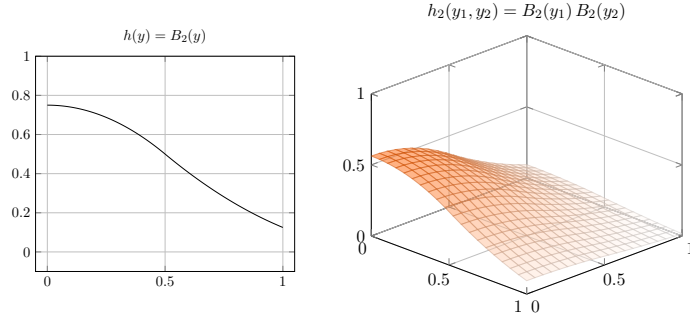


Figure 3.1: The univariate B-spline  $h(x) = B_2(x)$  and the two-dimensional tensor product B-spline  $h_1(x_1, x_2) = B_2(x_1) B_2(x_2)$ .

### 3 Numerics

We define a shifted, scaled and dilated B-spline  $B_2 \in \mathcal{C}^1([0, 1])$  as

$$B_2(x) := \begin{cases} -x^2 + \frac{3}{4} & \text{for } 0 \leq x < \frac{1}{2}, \\ \frac{1}{2} (x^2 - 3x + \frac{9}{4}) & \text{for } \frac{1}{2} \leq x \leq 1, \end{cases} \quad (3.1)$$

depicted in Figure 3.1, that was also used in [12, 11]. We approximate the tensor product B-spline

$$h(\mathbf{x}) = \prod_{j=1}^d B_2(x_j), \quad (3.2)$$

by the approximated Chebyshev, cosine or transformed Fourier partial sums  $S_I^\Lambda h$  given in (2.8), (2.13) and (2.19). We study the resulting relative  $\ell_2$  and  $\ell_\infty$  approximation errors

$$\varepsilon_p := \frac{\left\| (h(\mathbf{x}_j) - S_I^\Lambda h(\mathbf{x}_j))_{j=1}^R \right\|_{\ell_p}}{\left\| (h(\mathbf{x}_j))_{j=1}^R \right\|_{\ell_p}}, \quad p \in \{2, \infty\}, \quad (3.3)$$

that are evaluated at  $R \in \mathbb{N}$  random points  $\mathbf{x}_j \sim \mathcal{U}([0, 1]^d)$ . The approximated coefficients appearing in the approximated partial sums (2.8), (2.13) and (2.19) are calculated by solving the corresponding systems (2.9), (2.14) or (2.20).

A prominent choice for the frequency sets  $I$  is the hyperbolic cross given by

$$I_N^d := \left\{ \mathbf{k} \in \mathbb{Z}^d : \prod_{\ell=1}^d \max(1, |k_\ell|) \leq N \right\}, \quad (3.4)$$

which is considered in the context of the Fourier approximation [16, 5] and transformed Fourier approximation. For the Chebyshev and Cosine approximation we consider only the first orthant of such a hyperbolic cross  $I_N^d \cap \mathbb{N}_0^d$ . We illustrate both frequency sets  $I_N^d$  and  $I_N^d \cap \mathbb{N}_0^d$  in dimension  $d = 2$  with  $N = 8$  in Figure 3.2.



Figure 3.2: The hyperbolic cross  $I_8^2$  (left) and its first quadrant  $I_8^2 \cap \mathbb{N}_0^2$  (right).

### 3.1 The numerics of $\ell_2$ -approximation

In [16, 3, 17] we find a broad discussion on the approximation error decay of function in the Sobolev space  $H^m(\mathbb{T}^d)$  of mixed dominated smoothness  $m \in \mathbb{N}_0$ . It was proven that there is a worst case upper error bound of the form  $\varepsilon_2 = \varepsilon_2(N, d) \lesssim N^{-m}(\log N)^{(d-1)/2}$ . In [11] we find conditions on the logarithmic and the error function transformation  $\psi(\circ, \boldsymbol{\eta})$ , given in (2.21) and (2.22), such that a certain degree of smoothness of given  $\mathcal{C}^m(\mathbb{T}^d)$ -function is preserved under composition and the resulting periodized function is at least in  $H^\ell(\mathbb{T}^d)$ ,  $\ell \leq m$  and for each  $\ell$  it was calculated how large the parameter  $\boldsymbol{\eta}$  has to be chosen. For the considered  $\mathcal{C}^1([0, 1])$ -function in (3.1) we need to choose  $\eta_j > 3$  in each component of  $\boldsymbol{\eta} = (\eta_1, \dots, \eta_d)^\top$  for both the logarithmic transformation (2.21) and the error function transformation (2.22) to guarantee that the smoothness of  $h$  is preserved by the corresponding transformed Fourier systems.

In dimensions  $d \in \{1, 2, 3\}$  we compare the discrete  $\ell_2$ -approximation error  $\varepsilon_2$ , given in (3.3), with  $R = 100.000$  uniformly distributed evaluation points for all of the previously introduced approximation approaches. We consider frequency sets  $I_N^d$  for all transformed Fourier system and  $I_N^d \cap \mathbb{N}_0^d$  for any other system with  $N = 1, \dots, 100$  each. We obtain an error decay of  $\varepsilon_2(N, d) \lesssim N^{-1}$  for the cosine system and both the log- and erf-transformed Fourier system with  $\boldsymbol{\eta} = 2$ . For the Chebyshev system, as well as for the log- and the erf-transformed Fourier system with  $\boldsymbol{\eta} = 4$ , we obtain an error decay of  $\varepsilon_2(N, d) \lesssim N^{-2.5}$ . The particular  $\ell_2$ -errors are shown in Figure 3.3. These experiments highlight how a sufficient increase of the parameter  $\boldsymbol{\eta}$  in these parameterized transformations  $\psi(\circ, \boldsymbol{\eta})$  improves the approximation error by preserving more smoothness of the initially given function.

We also obtain certain preasymptotic phenomena which are caused by the singularities at the boundary points of the tensored density  $\varrho$ . Each singular density weights the exponentials by certain finite values over the center of their domain, but diverge quickly near the bounds of the domain. In multiple dimensions these univariate singularities stack and push the undistorted information towards the center of the domain. Therefore, the underlying rank-1 lattice has to be very fine in high dimensions to be able to sample the essential information that is pushed towards the center of the domain. Consequentially, for larger parameter  $\boldsymbol{\eta}$  the errors  $\varepsilon_2(N, d)$  are at first worse for small  $N$  than the errors for smaller parameter  $\boldsymbol{\eta}$ , but eventually yield better approximation results once  $N$  is large enough.

### 3.2 The problems with $\ell_\infty$ -approximation

As derived in [11] and recalled in (2.16), the transformed Fourier system (2.17) for non-periodic functions is the result of applying an inverted change of variable  $\psi^{-1}(\circ, \boldsymbol{\eta})$  in the form

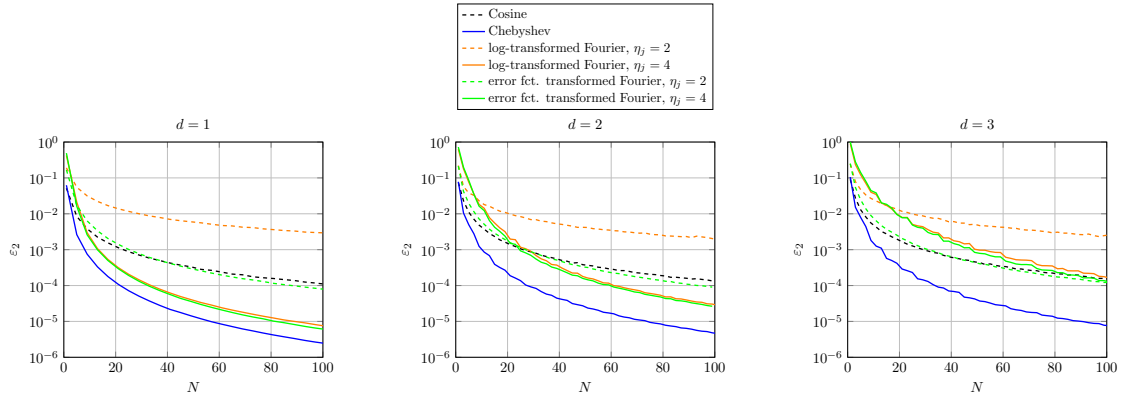


Figure 3.3: Comparison of the  $\ell_2$ -approximation error (3.3) in dimensions  $d \in \{1, 2, 3\}$  of the tensorized B-spline (3.1) being approximated by the cosine, Chebyshev and transformed Fourier system with the logarithmic transformation (2.21) and the error function transformation (2.22) with parameters  $\boldsymbol{\eta} = (\eta_j)_{j=1}^d, \eta_j \in \{2, 4\}$ .

of (2.15) to the Fourier system elements within the  $L_2(\mathbb{T}^d)$ -scalar product, in order to generate another orthonormal system in a given space  $L_{2,\omega}([-\frac{1}{2}, \frac{1}{2}]^d)$ . There are two interpretations for the resulting integral of the form

$$\int_{[0,1]^d} \frac{\varrho(\mathbf{y}, \boldsymbol{\eta})}{\omega(\mathbf{x})} e^{2\pi i(\mathbf{k}-\mathbf{m})\psi^{-1}(\mathbf{y}, \boldsymbol{\eta})} \omega(\mathbf{x}) \, d\mathbf{y} = \int_{\mathbb{T}^d} e^{2\pi i(\mathbf{k}-\mathbf{m})\mathbf{x}} \, d\mathbf{x} = \delta_{\mathbf{k}, \mathbf{m}}. \quad (3.5)$$

We either have another periodic system of the form  $\left\{ e^{2\pi i \mathbf{k} \cdot \psi^{-1}(\circ, \boldsymbol{\eta})} \right\}_{\mathbf{k} \in I}$  and the weighted  $L_{2,\varrho}([-\frac{1}{2}, \frac{1}{2}]^d)$ -scalar product; or we attach  $\sqrt{\varrho(\circ, \boldsymbol{\eta})/\omega(\circ)}$  to the individual exponentials  $e^{2\pi i \mathbf{k} \cdot \psi^{-1}(\circ, \boldsymbol{\eta})}$  and end up with the non-periodic system (2.17) and the originally given weighted  $L_{2,\omega}([-\frac{1}{2}, \frac{1}{2}]^d)$ -scalar product. If we consider a constant weight function  $\omega \equiv 1$ , then there is a drawback that comes with the later choice, because  $\varrho$  is unbounded and causes singularities at the boundary points of the elements in the approximated transformed Fourier sum (2.19). So, the pointwise approximation error  $\varepsilon_\infty$  in (3.3) isn't finite, unless we consider a suitably weighted  $\ell_\infty$ -norm that counteracts the behavior of the approximant towards the boundary points, which is discussed more thoroughly in [10, 11]. This strategy is based on choosing the weight function  $\omega$  in such a way that the quotient  $\varrho(\circ, \boldsymbol{\eta})/\omega(\circ)$  is either constant or converges at the boundary points. However, for any chosen torus-to-cube transformation - especially for the presented parameterized transformations  $\psi(\circ, \boldsymbol{\eta})$  in (2.21) and (2.22) with a fixed parameter  $\boldsymbol{\eta}$  - the weight function has to be chosen in such a way so that on one hand the singularities of the density function are controlled and on the other hand the given function  $h$  is still in  $L_{2,\omega}([0,1]^d)$ . We achieve this effect for example by choosing  $\psi(\mathbf{x}) = \psi(\mathbf{x}, \boldsymbol{\eta})$  to be the Chebyshev transformation (2.6), so that  $\varrho(\mathbf{x}) = \prod_{j=1}^d \frac{2}{\pi \sqrt{4x_j(1-x_j)}}$  is the usual unbounded Chebyshev weight. By putting  $\omega(\mathbf{x}) = \varrho(\mathbf{x})$  the quotient  $\varrho(\circ, \boldsymbol{\eta})/\omega(\circ)$  is constant. We end up with the same weighted  $L_{2,\omega}$ -scalar product as in the Chebyshev system and the real part of the resulting transformed Fourier system is (up to a constant) a subset of the Chebyshev system (2.5).

## 4 Conclusion

We considered the approximation of non-periodic functions on the cube  $[0, 1]^d$  by different systems of orthonormal functions. We compared the Chebyshev system that is orthonormal with respect to a weighted  $L_2$ -scalar product, the system of half-periodic cosines that uses tent-transformed sampling nodes and a parameterized transformed Fourier system. For the cosine system, which basically only mirrors a non-periodic function at its boundary points, as well as the transformed Fourier system with a small parameter, yielded the worst approximation errors. Switching to the Chebyshev system, which mirrors and additionally smoothens a given function, improved the approximation error decay. The same effect was obtained for the transformed Fourier system after increasing the parameter enough to obtain a better smoothing effect. The numerical experiments showcased the proposed parameter control in [11] that is set up by periodizing functions via families of parameterized torus-to-cube mappings. This approach in particular generalizes the idea used to derive Chebyshev polynomials.

## References

- [1] L. Bos, M. Caliari, S. De Marchi, M. Vianello, and Y. Xu. Bivariate lagrange interpolation at the padua points: The generating curve approach. *Journal of Approximation Theory*, 143, 11 2006.
- [2] J. P. Boyd. *Chebyshev and Fourier Spectral Methods*. Dover Press, New York, NY, USA, second edition, 2000.
- [3] G. Byrenheid, L. Kämmerer, T. Ullrich, and T. Volkmer. Tight error bounds for rank-1 lattice sampling in spaces of hybrid mixed smoothness. *Numer. Math.*, 136:993–1034, 2017.
- [4] R. Cools, F. Y. Kuo, and D. Nuyens. Constructing lattice rules based on weighted degree of exactness and worst case error. *Computing*, 87:63–89, 2010.
- [5] D. Dūng, V. N. Temlyakov, and T. Ullrich. *Hyperbolic Cross Approximation*. Advanced Courses in Mathematics – CRM Barcelona. Birkhäuser, Cham, 2018.
- [6] P. Dencker and W. Erb. Multivariate polynomial interpolation on lissajous-chebyshev nodes. *J. Approx. Theory*, 219:15–45, 2017.
- [7] A. Iserles and S. Norsett. From high oscillation to rapid approximation I: Modified fourier expansions. *Ima Journal of Numerical Analysis - IMA J NUMER ANAL*, 28:862–887, 02 2008.
- [8] L. Kämmerer. *High Dimensional Fast Fourier Transform Based on Rank-1 Lattice Sampling*. Dissertation. Universitätsverlag Chemnitz, 2014.
- [9] F. Y. Kuo, G. Migliorati, F. Nobile, and D. Nuyens. Function integration, reconstruction and approximation using rank-1 lattices. *Math. Comput.*, 2020. to appear.
- [10] R. Nasdala and D. Potts. Transformed rank-1 lattices for high-dimensional approximation. *Electron. Trans. Numer. Anal.*, 53:239–282, 2020.
- [11] R. Nasdala and D. Potts. Efficient multivariate approximation on the cube. *Numer. Math.*, 2021. doi: 10.1007/s00211-021-01177-9.

- [12] D. Potts and T. Volkmer. Fast and exact reconstruction of arbitrary multivariate algebraic polynomials in Chebyshev form. In *11th international conference on Sampling Theory and Applications (SampTA 2015)*, pages 392–396, 2015.
- [13] J. Shen, T. Tang, and L.-L. Wang. *Spectral Methods*, volume 41 of *Springer Ser. Comput. Math.* Springer-Verlag Berlin Heidelberg, Berlin, 2011.
- [14] I. H. Sloan and P. J. Kachoyan. Lattice methods for multiple integration: Theory, error analysis and examples. *SIAM J. Numer. Anal.*, 24:116–128, 1987.
- [15] G. Suryanarayana, D. Nuyens, and R. Cools. Reconstruction and collocation of a class of non-periodic functions by sampling along tent-transformed rank-1 lattices. *J. Fourier Anal. Appl.*, 22:187–214, 2016.
- [16] V. N. Temlyakov. Reconstruction of periodic functions of several variables from the values at the nodes of number-theoretic nets. *Anal. Math.*, 12:287–305, 1986. In Russian.
- [17] T. Volkmer. *Multivariate Approximation and High-Dimensional Sparse FFT Based on Rank-1 Lattice Sampling*. Dissertation. Universitätsverlag Chemnitz, 2017.